Response to Reviewer #1

Manuscript: A computationally efficient TVD-FFSL hybrid tracer transport scheme on spherical centroidal Voronoi tessellations in iAMAS (v2.6.3)

Journal: Geoscientific Model Development (GMD)

Authors: Gudongze Li et al.
Corresponding author: Chun Zhao (chunzhao@ustc.edu.cn)

Response to Reviewer #1

General Comment:

> *The authors describe a 3D transport scheme for the IAMAS model that employs a nominally 2nd-order TVD scheme for horizontal transport on the horizontal SCVT meshes and a PPM based FFSL scheme for vertical transport. The scheme is of potential interest to users of IAMAS and perhaps other models that employ icosahedral meshes or SCVT meshes. There are two main areas that need attention in the current manuscript to allow readers to evaluate the effectiveness of the authors' new scheme. The first area regards the description and properties of the scheme. The second concerns the performance of the horizontal TVD scheme and comparison of results from the new scheme with published results from other schemes.*

Response:

We sincerely thank the reviewer for insightful evaluation. The reviewer's exceptionally constructive feedback has helped us identify oversights in our initial experimental setup, substantially improving the scientific rigor of our manuscript. In response, we have refined our terminology, replacing strict claims of "monotonicity" with "approximately shape-preserving" to ensure scientific accuracy. Furthermore, we have re-conducted all 2D idealized experiments in Section. 3 under updated configurations, updating all figures, error norms, and discussions in the Section. 3 and Supplementary Material. As condensed in our revised 2D summary, although TVD-FFSL relaxes strict monotonicity, it maintains robust approximate shape preservation and accuracy strictly comparable to 2H1FCT, with minor extrema variations easily managed via mass-conserving clipping. Overall, the updated results confirm that TVD-FFSL achieves a highly practical balance, delivering high computational efficiency at high resolutions while maintaining sufficient numerical precision for atmospheric transport. Detailed point-by-point responses to each comment are provided below.

Comment 1:

> *Concerning the formulation and properties of the 3D scheme:*
>
> *What is the integration procedure for the full 3D scheme that combines the horizontal TVD scheme and the vertical PPM-based FFSL scheme? For the horizontal TVD scheme, the*

authors present the integration in equation (11):

$$\bar{\rho\psi}^{(1)} = \bar{\rho\psi}^{n} + \Delta t\, \mathbf{L}(\bar{\rho\psi}^{n})$$
$$\bar{\rho\psi}^{n+1} = \tfrac{1}{2}\bar{\rho\psi}^{n} + \tfrac{1}{2}\bar{\rho\psi}^{(1)} + \tfrac{1}{2}\Delta t\, \mathbf{L}(\bar{\rho\psi}^{(1)}) \quad (11)$$

If we denote the vertical scheme operator as P, the question is how is it combined with the scheme (11)? One possibility is

$$\bar{\rho\psi}^{(1)} = \bar{\rho\psi}^{n} + \Delta t\, \mathbf{L}(\bar{\rho\psi}^{n}) + \Delta t\, \mathbf{P}(\bar{\rho\psi}^{n}),$$
$$\bar{\rho\psi}^{n+1} = \tfrac{1}{2}\bar{\rho\psi}^{n} + \tfrac{1}{2}\bar{\rho\psi}^{(1)} + \tfrac{1}{2}\Delta t\, \mathbf{L}(\bar{\rho\psi}^{(1)}) + \tfrac{1}{2}\Delta t\, \mathbf{P}(\bar{\rho\psi}^{n}).$$

One could imagine other variants, for example where the FFSL update is left out of the first step and the full FFSL update is included in the final TVD step, i.e.

$$\bar{\rho\psi}^{(1)} = \bar{\rho\psi}^{n} + \Delta t\, \mathbf{L}(\bar{\rho\psi}^{n}),$$
$$\bar{\rho\psi}^{n+1} = \tfrac{1}{2}\bar{\rho\psi}^{n} + \tfrac{1}{2}\bar{\rho\psi}^{(1)} + \tfrac{1}{2}\Delta t\, \mathbf{L}(\bar{\rho\psi}^{(1)}) + \Delta t\, \mathbf{P}(\bar{\rho\psi}^{n}).$$

The authors need to clearly state how the full 3D scheme is implemented.

Response:

We thank the reviewer for this important question. In our implementation, the horizontal operator **L** and the vertical operator **P** are combined into a single hybrid spatial operator and integrated in time using the second-order TVD Runge-Kutta method. Both **L** and **P** are therefore calculated at the same state within each Runge-Kutta sub-step. The equation and description of the TVD Runge-Kutta method in Section 2.2.3 have been revised as follows: "

$$\bar{\rho\psi}^{(1)} = \bar{\rho\psi}^{n} + \Delta t\, (\mathbf{L}(\bar{\rho\psi}^{n}) + \mathbf{P}(\bar{\rho\psi}^{n}))$$
$$\bar{\rho\psi}^{n+1} = \tfrac{1}{2}\bar{\rho\psi}^{n} + \tfrac{1}{2}\bar{\rho\psi}^{(1)} + \tfrac{1}{2}\Delta t\, (\mathbf{L}(\bar{\rho\psi}^{(1)}) + \mathbf{P}(\bar{\rho\psi}^{(1)})) \quad (11)$$

where **L** denotes the horizontal scheme operator and **P** denotes the vertical scheme operator."

Comment 2:

Is the limiter applied on both steps in (11) for the TVD scheme?

Response:

Yes, the limiter is applied in both steps of the TVD Runge-Kutta method. If the limiter is not applied in the horizontal TVD scheme (i.e., $r \equiv 1$), the scheme reduces to a second-order centered scheme which is unstable. To clarify this, we have added the following sentence to the Section 2.2.3: "The KOREN limiter is applied within **L** in both steps of the TVD Runge-Kutta method."

Comment 3:

The TVD schemes and the PPM-based FFSL scheme are derived and analyzed for one-dimensional transport, and usually they use some form of splitting to handle multi-dimensional

> *transport. Furthermore, the TVD scheme is usually a single-step scheme-the first step equation in (11). Presumably, the two-step time integration (11) renders the 2D scheme stable? Is the 2D scheme stable without the application of the limiter ($r \equiv 1$). Is the full 3D scheme stable without the limiters applied in the TVD scheme and the PPM scheme? Stability analyses are needed for (11) for the unlimited scheme (at least in 1D, ideally in 2D), and for the unlimited version of the full combined TVD- FFSL scheme, perhaps in 2D (x,z).*

Response:

Thanks for your important questions about time integration and limiter. We emphasize that even after correcting the experimental setup (see our response to Comment 6), the single-step TVD scheme is still unstable. The TVD Runge-Kutta method guarantees stability. With the time integration in Eq. 11, the scheme remains stable and preserves the cosine bell shape with low errors. We have updated the rationale at the start of Section 2.2.3 as follows: "Although TVD schemes conventionally use single-step time integration, our tests showed that this approach is unstable when applied to iAMAS meshes."

Regarding the stability of the unlimited scheme: when the limiter is disabled ($r \equiv 1$, i.e., $\phi \equiv 1$), the TVD reconstruction in Eq. 5 reduces to the second-order centered form $\psi_{(C,D)} = (\psi_C + \psi_D)/2$. A second-order centered advection scheme is linearly unstable. Therefore, without the limiter, the 2D horizontal scheme is unstable, and so is the full 3D TVD-FFSL scheme, since the horizontal operator is part of the combined operator. The limiter is thus essential for the stability of both schemes.

We have clarified the importance of the limiter in the revised manuscript. The following remark has been added right after Eq. 5: "Without the limiter ($\phi \equiv 1$), the reconstruction reduces to the second-order centered form $\psi_{(C,D)} = (\psi_C + \psi_D)/2$, which is linearly unstable for advection. The limiter is therefore indispensable for stability."

Comment 4:

> *Is the horizontal TVD scheme guaranteed to be TVD using the time integration (11)? If the scheme is not spatially split then the 1D analysis isn't conclusive.*

Response:

We sincerely thank the reviewer for pointing this out. We completely agree that the 1D TVD analysis is not strictly conclusive for a 2D unsplit scheme on an unstructured mesh.

As proven by Goodman and LeVeque (1985), any strict TVD scheme in two or more dimensions is limited to first-order accuracy. Therefore, because our horizontal spatial scheme is an unsplit multi-dimensional operator on SCVT meshes, it is not guaranteed to be strictly TVD. In our practical implementation, the term "TVD scheme" was used to indicate that the scheme employs 1D TVD-type limiters to suppress non-physical oscillations. In a multi-dimensional context, it is more rigorously defined as a approximately shape-preserving scheme rather than a strict TVD one.

We use the TVD Runge-Kutta time integration in Eq. 11 not to confer a strict TVD property on the horizontal scheme, but to ensure that the time-stepping itself does not amplify spurious oscillations (Gottlieb and Shu, 1998). In practice, we found that single-step explicit integration produced unstable results in standard tests. The second-order TVD-RK scheme (Eq. 11), by contrast, successfully suppresses these oscillations and yields competitive results.

To ensure mathematical rigor and avoid misleading the readers, we have carefully revised the relevant subsections (Section 2.2.1 and Section 2.2.3). For each entry below, the original wording is shown first, followed by the revised wording in green.

- **L174:** "Then, $\psi_{(C,D)}$ of a TVD scheme with flux limiter on unstructured grids is written as (Bruner et al., 1997; Darwish and Moukalled, 2003)" has been revised to "Then, $\psi_{(C,D)}$ of a monotonicity-preserving scheme using a TVD-type flux limiter on unstructured grids is written as (Bruner et al., 1997; Darwish and Moukalled, 2003)."

- **L193:** "While the theoretical framework above applies to one-dimensional uniform grids, verification through testing is required for two-dimensional SCVT meshes." has been revised to "The theoretical framework above applies to one-dimensional uniform grids. Furthermore, our two-dimensional scheme employing a TVD-type limiter on SCVT meshes is not strictly TVD (Goodman and LeVeque, 1985). Practical tests are therefore required to verify the shape-preserving properties of the scheme on two-dimensional SCVT meshes (See Sec. 3)."

- **L210:** "Consequently, the horizontal flux operator achieves theoretical monotonicity and second-order accuracy with improved computational efficiency." has been revised to "Consequently, the horizontal flux operator achieves approximately shape-preserving properties and nominal second-order accuracy with improved computational efficiency."

- **L249:** "When the spatial discretization scheme follows the TVD framework, TVD Runge-Kutta timestepping methods provide excellent compatibility and effectively avoid the oscillations that can arise from non-TVD Runge-Kutta schemes (Gottlieb and Shu, 1998). The TVD time integration preserves the monotonicity maintained by the horizontal discretization, ensuring as much as possible that the hybrid scheme remains TVD in both space and time." has been revised to "When the spatial discretization follows the TVD framework, TVD Runge-Kutta timestepping methods provide excellent compatibility. They preserve the approximately shape-preserving properties of both the horizontal and vertical operators without amplifying the spurious oscillations that arise from non-TVD Runge-Kutta schemes (Gottlieb and Shu, 1998). The combined scheme therefore remains approximately shape-preserving."

Comment 5:

> *Concerning the results and scheme performance:*
>
> *It is difficult to assess how well this TVD scheme performs in comparison to other published schemes. The authors use significantly smaller Courant numbers in their tests compared to results for other published scheme. For example, the existing IAMAS scheme comes from Skamarock and Gassman (2012). The phase errors for the authors' second- order scheme appear to be much less than those reported for the second order scheme considered in Skamarock and Gassman, however, the authors tests use much-lower Courant numbers and higher resolution than used to produce the results in Skamarock and Gassman. For example, compare the authors' figure 3 for the solid-body rotation test using the cosine bell with Skamarock and Gassman figure 3. Skamarock and Gassman use a nominally 240 km horizontal SCVT mesh for this test with a centerline Courant number of ∼0.58 (the bell is located over the equator), whereas the authors place the bell at 30N and use a much smaller time step (assuming the 6Δ rule the authors note earlier in the manuscript?) on a 60 km mesh with the resulting Courant number being ∼0.2. Are the lower Courant numbers and higher resolution used in the authors' tests the reason for the different error characteristics for their 2nd order scheme compared to Skamarock and Gassman, or does the different time integration used in the au-*

thors' new scheme result in significantly reduced phase errors (and now similar to the other higher-order published schemes). Test with higher Courant numbers and lower resolution are needed to answer this question and give readers the information needed to evaluate the scheme.

Response:

We thank the reviewer for this insightful comment. Following the reviewer's suggestion, we have repeated the solid body rotation, and deformational-flow tests with the time step and the mesh resolutions used in Skamarock and Gassman (2012). These tests also reflect a correction to the experimental setup, which is described in detail in our response to Comment 6. The initial centers of the cosine bell and slotted cylinder have also been relocated from 30°N to the equator to match the setup of Skamarock and Gassman (2012). Accordingly, the opening of Section 3 has been revised as follows:

"Following previous studies (Skamarock and Menchaca, 2010; Nair and Lauritzen, 2010; Skamarock and Gassmann, 2011; Dong et al., 2014; Lauritzen et al., 2014), three idealized 2D test cases are examined: solid body rotation, deformational flow and gaussian hills. Table 1 lists the mesh configurations and time steps used in these tests. The time step settings at different resolutions follow Table 1 of Skamarock and Gassmann (2011). All SCVT meshes are generated using the JIGSAW algorithm (Engwirda, 2017) rather than the traditional Lloyd algorithm (Renka, 1997), so the 2H1FCT results presented here may differ slightly from those in Skamarock and Gassmann (2011) due to mesh differences."

At 240 km with the matched time step, TVD-FFSL still exhibits reduced phase errors (Fig. S1) and smaller L2 errors ($L_2 = 0.2421$; Fig. 4) than the second-order scheme reported in Fig. 3 and 4 of Skamarock and Gassman (2012). For the cosine bell test, Lauritzen et al. (2014) regard an L2 error of 0.033 as the threshold for practical usability, and TVD-FFSL meets this threshold only at 60 km and finer resolutions (Fig. 4). The main focus of this study is to highlight the accuracy and computational efficiency of TVD-FFSL at relatively high resolutions, so the main text retains the 60 km results, while the U240km and U120km results are provided in the supplementary material (Fig. S1 and Fig. S2) for direct comparison with published results. After updating and correcting the experimental setup, the test results have also changed. The corresponding discussion in Section 3.1.1 has therefore been revised as follows:

"Fig. 3 displays the spatial distributions of the cosine bell after one full revolution at 60 km resolution. Visually, both the 2H1FCT and TVD-FFSL schemes accurately transport the tracer without noticeable phase errors or severe structural distortions. This resolution is the coarsest at which TVD-FFSL achieves an L_2 error below 0.033, the threshold for acceptable solution quality (Lauritzen et al., 2014). At coarser resolutions, such as 240 km and 120 km, TVD-FFSL has distorted structural symmetry (Fig. S1-2). At 60 km, however, the TVD-FFSL contours remain highly symmetric (Fig. 3c), confirming its approximate shape preservation. The 2H1FCT scheme achieves a maximum peak of 987.74 while strictly maintaining non-negativity due to its FCT limiter. The TVD-FFSL scheme yields a slightly lower peak (973.84), which is due to moderate numerical dissipation near local extrema introduced by the flux limiters. Unlike 2H1FCT, TVD-FFSL uses extrapolation-based slope reconstruction on SCVT grids and therefore does not strictly satisfy the TVD property. This produces a minor undershoot, with a minimum of -0.707 at 60 km resolution. The undershoot decreases with resolution, reaching -0.291 at 30 km.

To quantitatively evaluate the spatial accuracy of the transport schemes, the normalized L_2 and L_{inf} error norms are computed (see Appendix C). Both schemes exhibit a systematic reduction in errors as the resolution increases (Fig. 4). Overall, 2H1FCT yields lower error norms than TVD-FFSL at all resolutions. However, the errors of TVD-FFSL remain strictly within the same order of magnitude as 2H1FCT. Overall, both schemes sustain very similar asymptotic convergence behavior, approaching second-order accuracy under this test across the tested resolution range.”

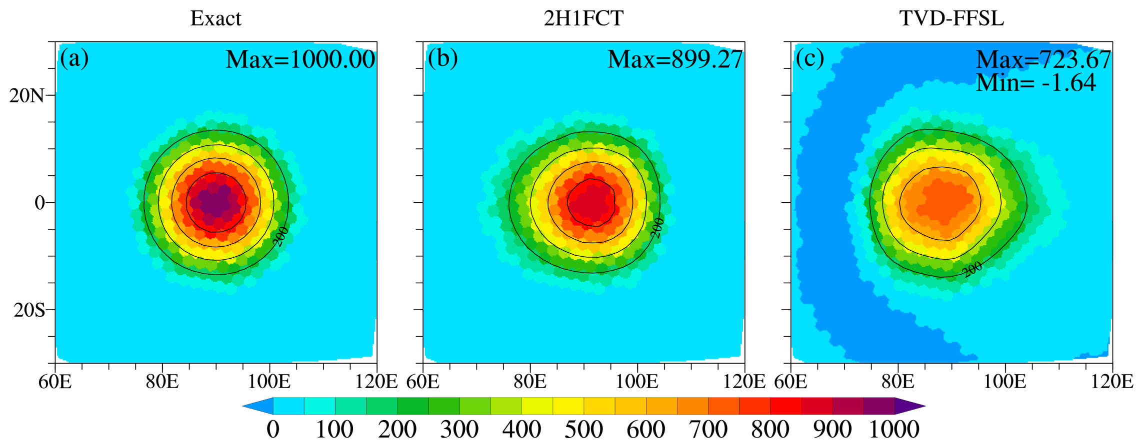

Figure S1. Cosine bell under the solid body rotation test on the U240km mesh at $t = T$. (**a**) Exact solution. (**b**) Result of the original 2H1FCT scheme in iAMAS. (**c**) Result of the TVD-FFSL hybrid scheme.

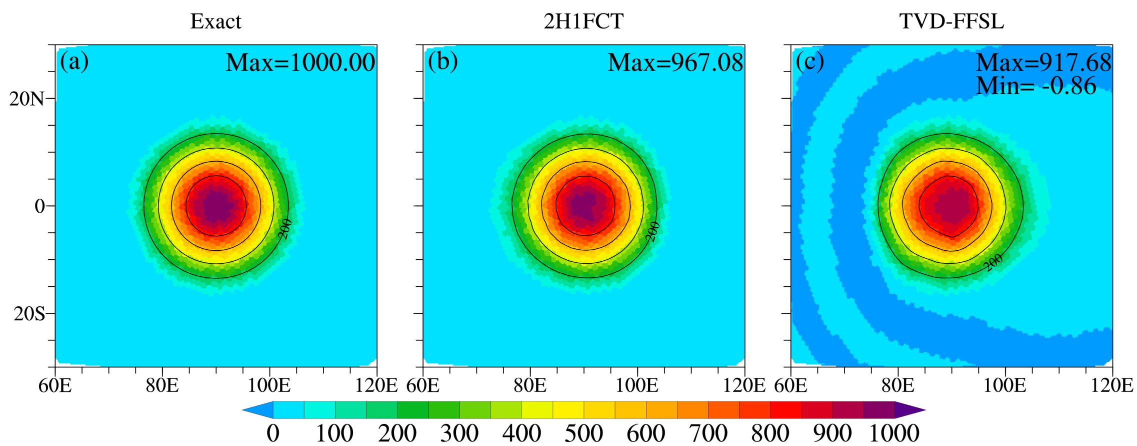

Figure S2. Cosine bell under the solid body rotation test on the U120km mesh at $t = T$. (**a**) Exact solution. (**b**) Result of the original 2H1FCT scheme in iAMAS. (**c**) Result of the TVD-FFSL hybrid scheme.

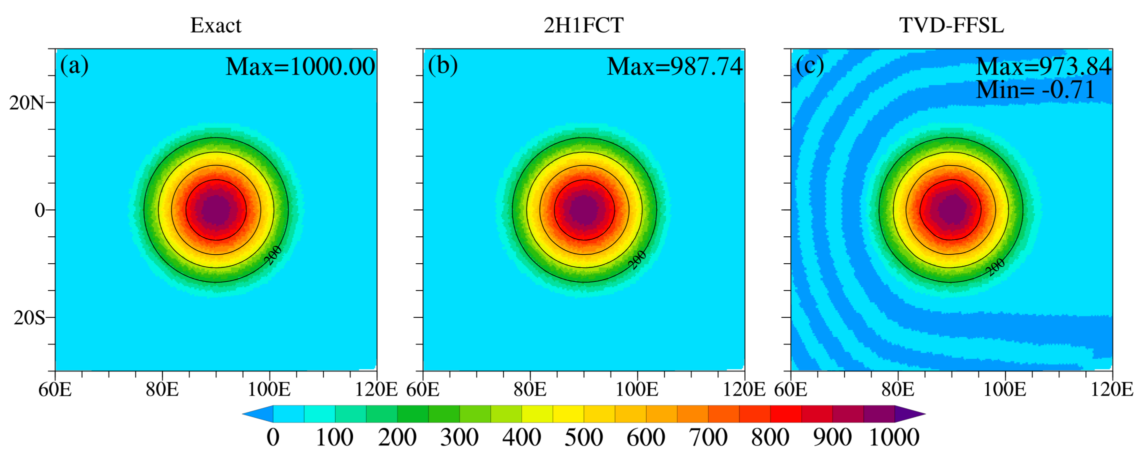

Figure 3. Cosine bell under the solid body rotation test on the U60km mesh at $t = T$. (**a**) Exact

solution. (**b**) Result of the original 2H1FCT scheme in iAMAS. (**c**) Result of the TVD-FFSL hybrid scheme.

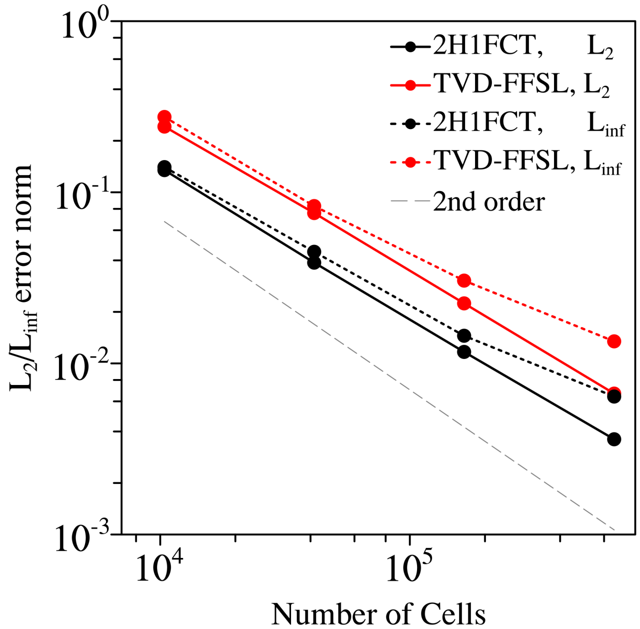

Figure 4. The L_2 and L_{inf} error norms of the cosine bell under the solid body rotation test.

With the new time step and mesh resolutions, results of the deformational-flow test have also changed. And the associated discussion in Section 3.2 has been updated as follows:

"We also test the smooth cosine bell initial condition under this scenario. Fig. 7 illustrates the time evolution of the cosine bell at $t = \frac{T}{4}, \frac{T}{2}, \frac{3T}{4}$ and $t = T$ for both the 2H1FCT and TVD-FFSL schemes. Both schemes accurately capture the strong stretching and shearing deformation. At $t = \frac{T}{4}$ and $t = \frac{3T}{4}$, the initial bell is intensely stretched. The TVD-FFSL scheme smoothly captures this filamentary structure without breaking it up into unphysical discrete blobs, demonstrating robust shape-preserving capabilities under strong deformation. Upon the flow reversal at $t = \frac{T}{2}$ and $t = T$, both schemes successfully recover the original bell shape. At $t = T$, 2H1FCT achieves a peak value of 980.81 while maintaining strict positivity. TVD-FFSL yields a slightly lower peak (976.81) due to flux limiter dissipation during intense deformation, alongside a negligible undershoot (-0.50).

Fig. 8 further illustrates the error norms of the cosine bell under deformational flow. The absolute values of both L_2 and L_{inf} error norms for the TVD-FFSL scheme are also slightly larger than those of the 2H1FCT scheme across scales (from 240 km to 30 km). However, as resolution is refined to 30 km, the L_{inf} error norm of TVD-FFSL converges to match that of 2H1FCT. Meanwhile, the L_2 error gap between the two schemes also narrows considerably at 30 km. As clearly demonstrated by the steeper slopes of the TVD-FFSL lines in Fig. 8, the TVD-FFSL scheme exhibits superior convergence properties in this case."

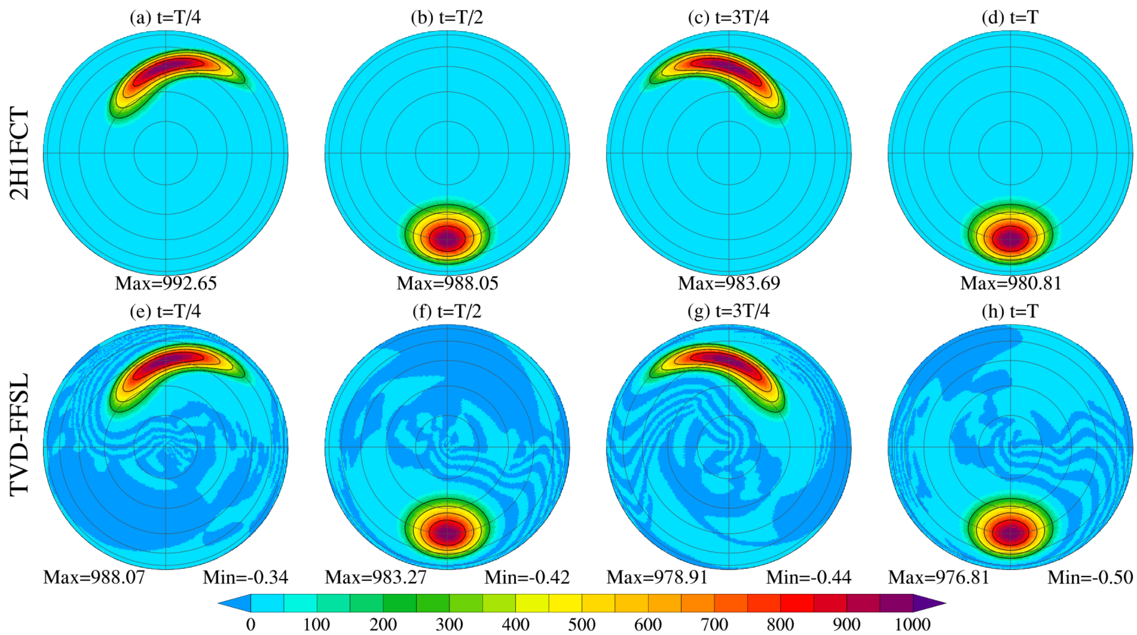

Figure 7. Cosine bell under deformational flow on the U60km mesh. (a-d) Results of 2H1FCT at $t = \frac{T}{4}, \frac{T}{2}, \frac{3T}{4}, T$. (e-h) Results of TVD-FFSL at $t = \frac{T}{4}, \frac{T}{2}, \frac{3T}{4}, T$.

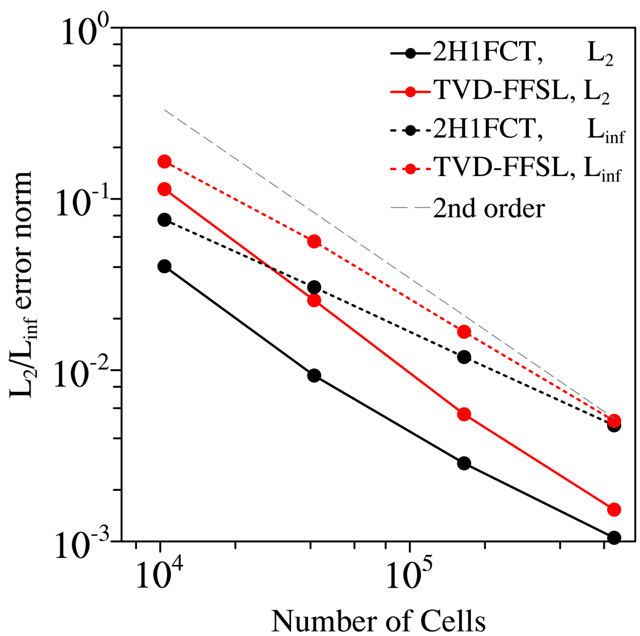

Figure 8. The L_2 and L_{inf} error norms of the cosine bell under deformational flow.

With the above test results updated and the new Gaussian hills test case added, the summary of the 2D idealized tests (Section 3.4) has also been revised as follows:

"The 2D idealized tests validate the horizontal TVD operator of the proposed TVD-FFSL hybrid scheme across diverse flow dynamics and tracer field smoothness levels on SCVT meshes. Under solid body rotation, the scheme demonstrates robust, approximately shape-preserving properties for both smooth and discontinuous initial conditions. Localized extrema violations near sharp interfaces remain minor ($\approx 1\%$ of the dynamic range) and can be easily rectified via mass-conserving clipping—a modest trade-off for bypassing the computationally expensive FCT step. In complex deformational flows, TVD-FFSL accurately resolves filamentary structures without unphysical fragmentation. For smooth distributions, the scheme exhibits good peak retention and resolution-dependent undershoot elimination, recovering non-negativity once the grid spacing enters the well-resolved regime (60 km). While nonlinear flux limiting near strong shear interfaces induces sub-second-order asymptotic convergence, TVD-FFSL maintains error norms within the same order of magnitude as 2H1FCT across all scales, converging to virtually identical L_2 and L_∞ errors at high resolutions (30 km). These results confirm that the horizontal TVD component meets the requirements for accurate and reliable atmospheric transport."

Comment 6:

> *Why does the 2HIFCT scheme show overshoots (values greater than 1000) in Figure 5 for the slotted cylinder test problem? The results in Skamarock and Gassman (2012) do not show these overshoots (see Skamarock and Gassman figure 12) - the FCT limiter should eliminate all overshoots and undershoots. One possibility is that the discrete flow field is not divergence free (it is divergence free in the Skamarock and Gassman tests).*

Response:

We are sincerely grateful to the reviewer for this exceptionally careful and critical observation. The reviewer's remark pointed us directly to two oversights in our test setup that we had overlooked, and correcting them has materially improved the reliability of our results.

Upon investigation, we traced the unphysical overshoots of the 2H1FCT scheme to two causes:

a. The velocity field used in the original soild-body rotation test was defined through an analytical function inherited from the demonstration phase of the model, and it is not discretely divergence-free on the SCVT mesh. We have replaced it with a stream-function-based definition that is divergence-free by construction.

b. In the iAMAS test environment, the density field was slightly non-uniform owing to layer-thickness variations. We have corrected the setup to use a uniform density field.

After both corrections, the 2H1FCT results are free of overshoots and undershoots, apart from floating-point-roundoff-level deviations of magnitude smaller than 10^{-10} (Fig. 5b). Meanwhile, experimental results have also changed so that Section 3.1.2 has been updated as follows:

"Fig. 5b and Fig. 5c show the slotted cylinder distributions after one revolution at 60 km resolution, simulated by the 2H1FCT and TVD-FFSL schemes, respectively. Both schemes well maintain the global cylinder geometry and the narrow central slot. At a coarser 120 km resolution (Fig. S3), numerical diffusion induces noticeable slot smearing, consistent with results in Skamarock et al. (2012). However, grid refinement to 60 km effectively sharpens boundary definitions. The global extrema highlight the distinct limiting mechanisms of the two schemes. While 2H1FCT preserves the initial range (0.00–1000.00), TVD-FFSL exhibits a slight overshoot to 1012.77 and undershoot to -9.27 at 60 km. The sharp step discontinuity produces steeper reconstructed gradients, leading to larger extrema than in the smooth cosine bell case. Nevertheless, these oscillations remain minor ($\approx 1\%$ of the dynamic range) and spatially confined. In practice, they are removed by negative-value clipping with mass rescaling across local meshes, ensuring positivity and mass conservation.

The error norms for the slotted cylinder test are shown in Fig. 6. With discontinuous initial conditions, error characteristics differ markedly from smooth fields. The L_{inf} errors remain resolution-independent, as expected for transport of discontinuous fields. Numerical diffusion inherently smears sharp edges, causing errors that persist regardless of grid spacing. Conversely, L_2 errors decrease systematically with grid refinement. TVD-FFSL exhibits L_2 errors closely comparable to 2H1FCT across all resolutions, confirming its robust shape preservation under severe non-smooth conditions without requiring computationally expensive FCT limiters."

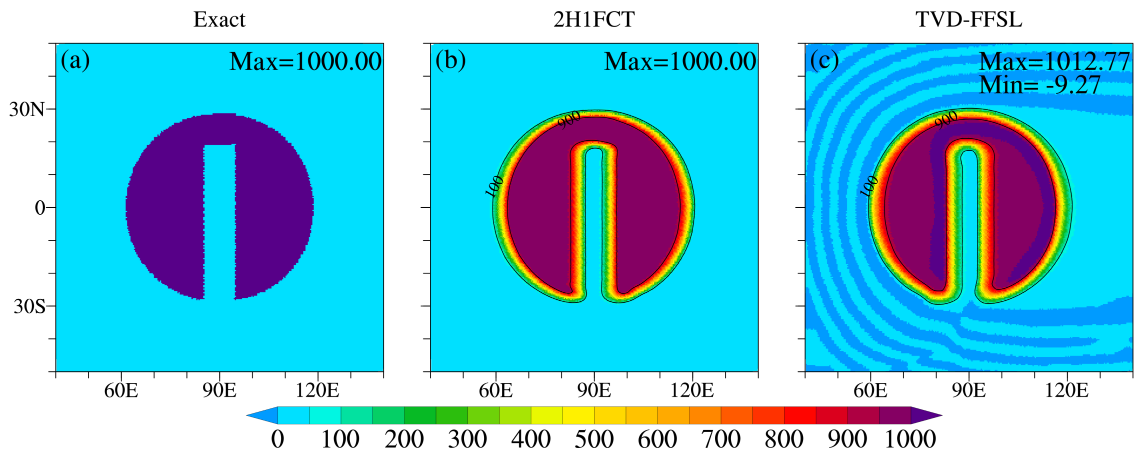

Figure 5. Slotted cylinder under the solid body rotation test on the U60km mesh at $t = T$. (**a**) Exact solution. (**b**) Result of the original 2H1FCT scheme in iAMAS. (**c**) Result of the TVD-FFSL hybrid scheme.

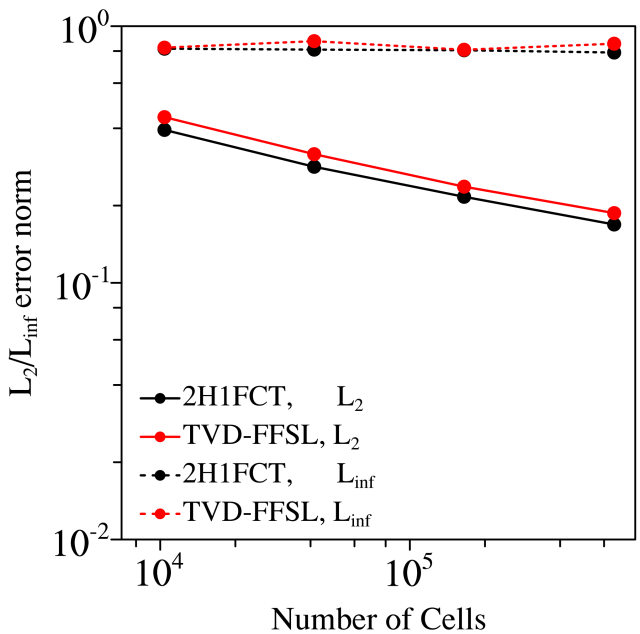

Figure 6. The L_2 and L_{inf} error norms of the slotted cylinder under the solid body rotation test.

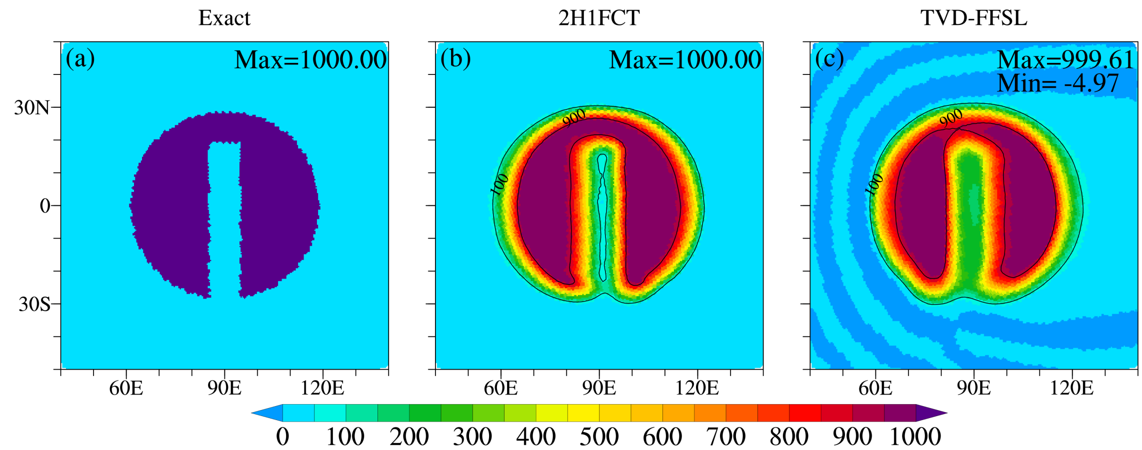

Figure S3. Slotted cylinder under the solid body rotation test on the U120km mesh at $t = T$. (**a**) Exact solution. (**b**) Result of the original 2H1FCT scheme in iAMAS. (**c**) Result of the TVD-FFSL hybrid scheme.

Comment 7:

> *Why are the TVD results and the 2HIFCT results shown in figure 5 positive definite but not monotonic (they contain overshoots)? If a nonzero constant value were added to the state would undershoots appear?*

Response:

Following the corrections described in our response to Comment 6, the 2H1FCT scheme is now monotone, with neither overshoots nor undershoots in the slotted cylinder test. We take this opportunity to clarify a point that directly addresses the reviewer's question.

In the actual implementation, both the 2H1FCT and the TVD-FFSL schemes apply a negative-value truncation (forced positivity) to the transported tracers, as a safeguard against accidental negative values that would crash the physical/chemical parameterizations downstream. This truncation is also the reason why, under the previous setup, the results exhibited overshoots but no undershoots.

As discussed earlier, the TVD-FFSL scheme is not strictly shape-preserving. At discontinuities, such as the edge of the cosine bell or the sharp corners of the slotted cylinder, it can produce small overshoots or undershoots. To prevent these tiny undershoots from destabilizing the parameterizations, they can be removed by the negative-value truncation combined with a local-mesh total-mass compensation that preserves global mass. In the revised manuscript, the TVD-FFSL results are presented without this truncation, so that the raw output of the scheme and its approximate shape-preservation behavior are fully visible.

We note that these overshoot and undershoot phenomena are confined to discontinuous regions. For smooth distributions, such as the Gaussian hills test, TVD-FFSL produces no undershoot even when the field minimum is a small positive value, since the limiter operates in its high-accuracy regime and the reconstruction stays within bounds (See details in response to Comment 8).

Comment 8:

The scheme convergence rates for the cosine bell test case are computed with the limiters on (figures 4 and 8). The less than 2nd-order convergence is caused by the limiters but may also be caused by the cosine bell being only only C1 continuous. The authors should report results with both limiters on and off for test cases using a continuous function such as the Gaussian hills test cases reported in Lauritzen et al (2014) - doi:10.5194/gmd-7-105-2014.

Response:

We thank the reviewer for this insightful suggestion. As discussed in our response to Comment 3, the KOREN limiter cannot be disabled in our scheme: without it, the TVD reconstruction reduces to an unstable second-order centered scheme. We therefore cannot directly report limiter-off results.

However, following the reviewer's suggestion, we have added the Gaussian hills test (Section 3.3) using the Case-2 deformational flow field from Nair and Lauritzen (2010). Despite the infinitely smooth (C^∞) initial condition, which removes the smoothness limitation of the cosine bell, the convergence rates of 2H1FCT remain sub-second-order on this test as well. We emphasize that the 2H1FCT results reported here were obtained directly from the unmodified MPAS-A v7 dynamical core source code, so this sub-second-order behaviour is what the scheme actually produces in our test environment rather than an artifact of our implementation. This indicates that, within our test environment, the limiter does contribute to the convergence-order reduction, even on smooth distributions. Nevertheless, the absolute error norm values across all our test cases are comparable to those reported in Skamarock and Gassmann (2011). The sub-second-order convergence on the Gaussian hills test may partly stem from differences in mesh generation (JIGSAW versus the Lloyd algorithm used by Skamarock) or from a stronger wind speed in our setup, as suggested by the more pronounced deformation of the tracer field. Regardless of the exact cause, the results confirm that TVD-FFSL achieves accuracy within the usable range at high resolutions (60 km and finer).

The results of Gaussian hills test case has been added as Section 3.3 as follows:

"The Gaussian hills test (Lauritzen et al. 2014) features an infinitely smooth (C^∞) initial condition, allowing the convergence rates of the transport schemes to be assessed without being limited by the smoothness of the initial condition. The initial condition follows Eq. 10 of Nair and Lauritzen (2010), with $b_0 = 5.0$ and $h_{\max} = 1000.0$. The two hills are centered at $(\lambda, \theta) = \left(\frac{5\pi}{6}, 0\right)$ and $\left(\frac{7\pi}{6}, 0\right)$ whose distribution is shown in Fig. S4. The deformational flow field follows Case-2 of Nair and Lauritzen (2010), hereafter referred to as the Nair-Case2 flow, adapted from the unit sphere to Earth's radius. Its stream function is:

$$\Psi(\lambda, \theta) = kR_e \sin^2(\lambda) \cos^2(\theta) \cos\left(\frac{\pi t}{T}\right) \tag{1}$$

where λ and θ denote longitude and latitude, respectively. The parameter $k = 75$ is chosen to maintain a Courant number comparable to that of the preceding idealized tests, with a flow period of $T = 12$ days.

Fig. 9 depicts the tracer fields at maximum deformation ($t = \frac{T}{2}$) and after full reversal ($t = T$) at 60 km resolution. At $t = \frac{T}{2}$, the flow stretches the twin hills into thin, swirling spiral filaments wrapping around the sphere. At 60 km, both schemes resolve these features without structural distortion and cleanly reconstruct the original shape. At coarser resolutions, such as 120 km, TVD-FFSL exhibits minor background undershoots (Fig. S5c–d). These disappear entirely at 60 km (Fig. 9c–d), where the computed minimum (1.582×10^{-5}) is close to the initial minimum on the same mesh (1.574×10^{-5}). This resolution-dependent elimination of undershoots on smooth distributions highlights the effective shape-preservation of TVD-FFSL once grid spacing enters the well-resolved regime. Furthermore, TVD-FFSL yields maximum values of 990.22 at $t = \frac{T}{2}$

and 980.04 at $t = T$, outperforming 2H1FCT (986.83 and 978.93, respectively) owing to reduced numerical dissipation along smooth gradients.

Driven by non-linear flux limiting near sharp gradients and filaments, both schemes exhibit sub-second-order asymptotic convergence rates rather than their theoretical convergence order (Fig. 10). Although 2H1FCT maintains lower error norms on coarse meshes, the discrepancy rapidly diminishes with grid refinement. At the finest resolution (30 km), the L_2 and L_{inf} error norms of TVD-FFSL converge to be virtually identical to those of 2H1FCT, with TVD-FFSL achieving a slightly lower L_{inf} error. These quantitative results confirm that TVD-FFSL achieves accuracy comparable to 2H1FCT and robust shape preservation at high resolutions for smooth distributions under deformational flow."

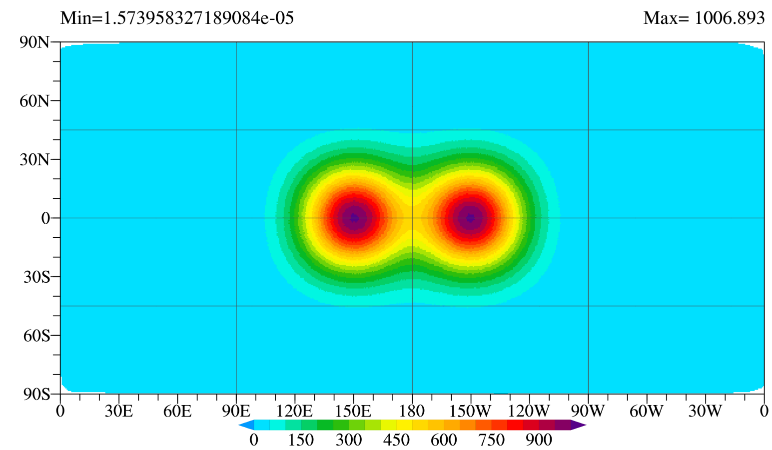

Figure S4. The initial condition of Gaussian hills test on the U60km mesh.

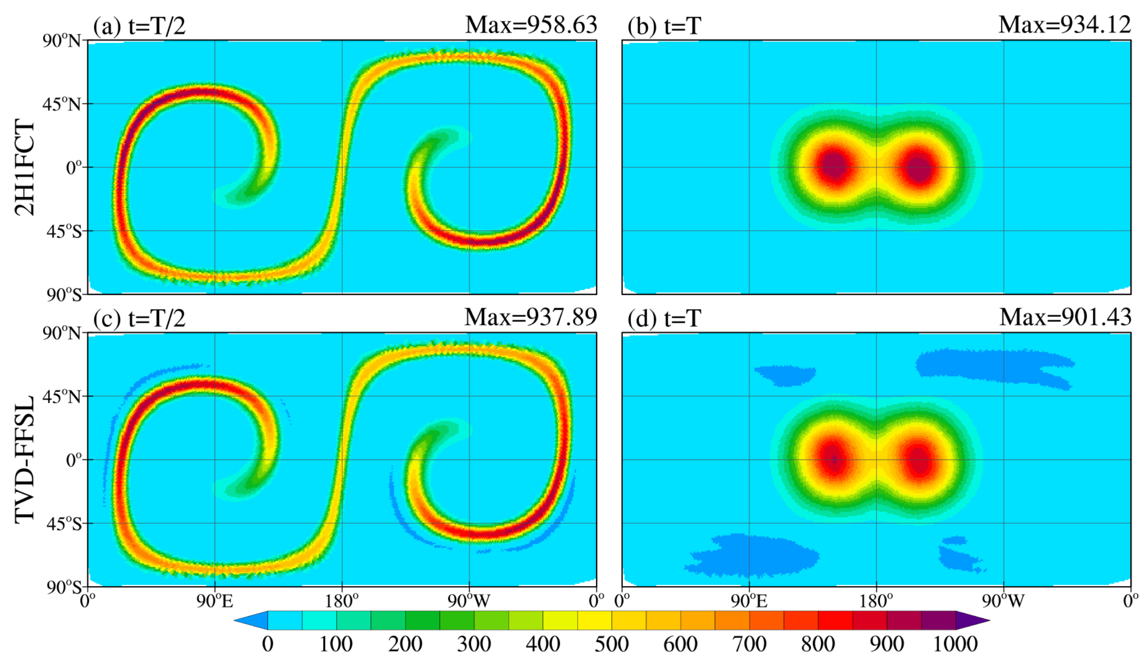

Figure S5. Gaussian hills under the Nair-Case2 deformational flow on the U120km mesh. (a-b) Results of 2H1FCT at $t = \frac{T}{2}, T$. (c-d) Results of TVD-FFSL at $t = \frac{T}{2}, T$.

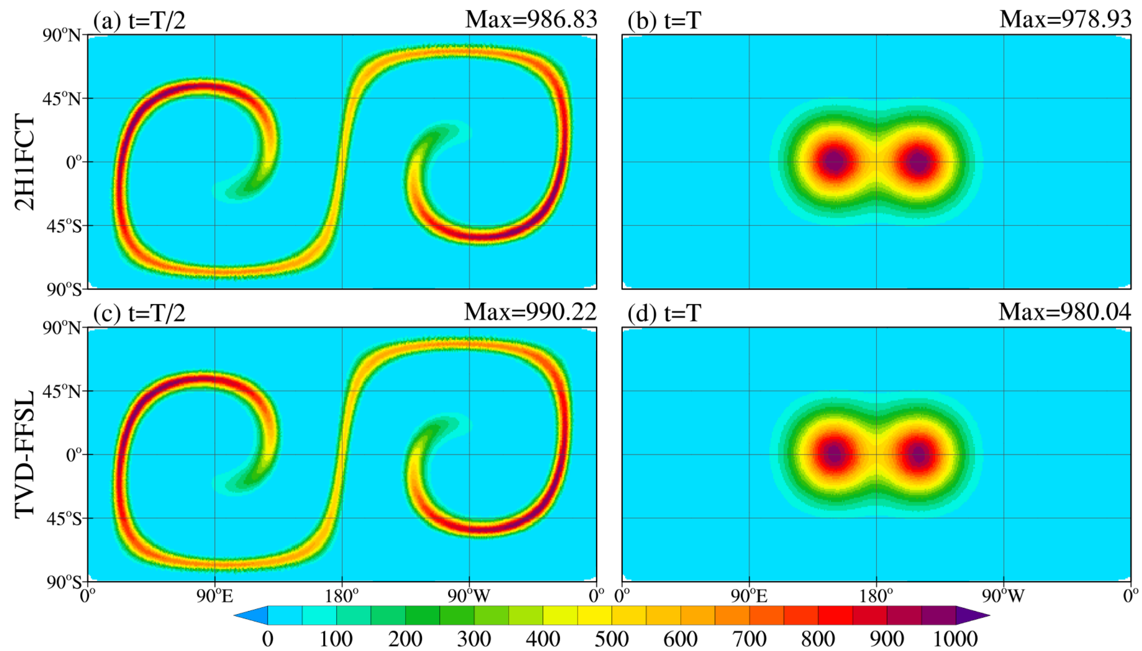

Figure 9. Gaussian hills under the Nair-Case2 deformational flow on the U60km mesh. (a-b) Results of 2H1FCT at $t = \frac{T}{2}, T$. (c-d) Results of TVD-FFSL at $t = \frac{T}{2}, T$.

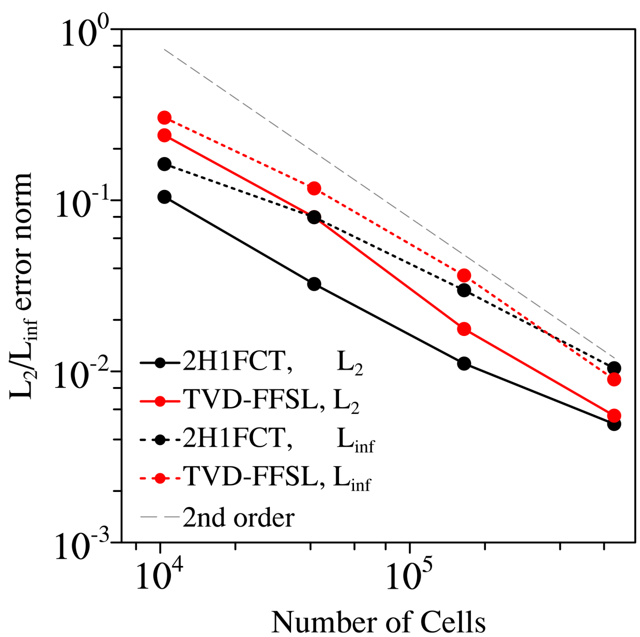

Figure 10. The L_2 and L_{inf} error norms of the Gaussian hills under the Nair-Case2 deformational flow.